Variational Phase-Amplitude Coupling Characterizes Signatures of Anterior Cortex Under Emotional Processing

Chuting Zhang, *Student Member, IEEE*, Chien-Hung Yeh, *Senior Member, IEEE*, and Wenbin Shi, *Member, IEEE*

***Abstract*—Emotion, an essential aspect in inferring human psychological states, is featured by entangled oscillators operating at multiple frequencies and montages. However, the dynamics of mutual interactions among rhythmic activities in EEGs under various emotional expressions are unclear. To this end, a novel method named variational phase-amplitude coupling is proposed to quantify the rhythmic nesting structure in EEGs under emotional processing. The proposed algorithm lies in variational mode decomposition, featured by its robustness to noise artifacts and its merit in avoiding the mode-mixing problem. This novel method reduces the risk of spurious coupling compared to that with ensemble empirical mode decomposition or iterative filter when evaluated by simulations. An atlas of cross-couplings in EEGs under eight emotional processing is established. Mainly, α activity in the anterior frontal region serves as a critical sign for neutral emotional state, whereas γ amplitude seems to be linked with both positive and negative emotional states. Moreover, for those γ-amplitude-related couplings under neutral emotional state, the frontal lobe is associated with lower phase-given frequencies while the central lobe is attached to higher ones. The γ-amplitude-related coupling in EEGs is a promising biomarker for recognizing mental states. We recommend our method as an effective tool in characterizing the entangled multifrequency rhythms in brain signals for emotion neuromodulation.**

***Index Terms*—Phase-amplitude coupling, variational mode decomposition, EEG, emotions, γ amplitude.**

Manuscript received 8 September 2022; revised 28 December 2022; accepted 5 February 2023. Date of publication 8 February 2023; date of current version 5 April 2023. This work was supported in part by the National Natural Science Foundation of China under Grants 62001026 and 62171028, and in part by the BIT High-Level Fellow Research Fund Program under Grant 3050012222022. *(Chuting Zhang and Chien-Hung Yeh contributed equally to this work.) (Corresponding author: Wenbin Shi.)*

Chuting Zhang and Wenbin Shi are with the School of Information and Electronics, Beijing Institute of Technology, Beijing 100081, China (e-mail: time_ting@126.com; swb1123@163.com).

Chien-Hung Yeh is with the School of Information and Electronics, Beijing Institute of Technology, Beijing 100081, China, and also with the Division of Interdisciplinary Medicine and Biotechnology, Beth Israel Deaconess Medical Center/Harvard Medical School, Boston, MA 02215 USA (e-mail: nzdiw1120@gmail.com).

This article has supplementary downloadable material available at https://doi.org/10.1109/JBHI.2023.3243275, provided by the authors.

Digital Object Identifier 10.1109/JBHI.2023.3243275

I. Introduction

EMOTIONS characterize a person's attitude toward and reflection on an objective event, which have a great effect on our life/health. As an illustration, chronic anxiety can easily affect sleep or even account for mental illness. Understanding the mechanism of emotional regulation is essential to develop reliable and effective emotion recognition tools that favor implementation in multiple fields, including education, medicine, and the military. Some researchers built emotional models to depict emotions with supportive quantitative references [1]. For example, the discrete model and dimensional model could be the two most widely referenced emotional models. The discrete model lies in the six basic emotions of happiness, sadness, anger, fear, surprise, and disgust, and was proposed by Ekman et al. [2]. Such a model is simple and intuitive in classification but fails to distinguish subtle changes in emotions. The dimensional model, on the other hand, divides the emotional space into two dimensions of valence-arousal (VA) as per cognitive evaluation, which was first introduced by Russell [3], wherein the two variables, i.e., valence and arousal, correspond to evaluations of negative/positive and high/low reactions to affective states. Later, the valence-arousal-dominance (VAD) model was introduced to expand the VA model with an additional dimension in dominance, measuring the controllability of emotion [4]. In the present study, eight discrete emotions were divided into three emotional states, with valence higher and lower than three being positive and negative, respectively. Since the valence of calmness is approaching three (positive/negative threshold), thus calmness is classified as a neutral emotional state.

More studies have investigated the dynamics of emotions with changing factors, such as brain regions and/or frequency band power. In 2009, Pessoa [5] revealed that the prefrontal lobe was involved in information transfer, directing attention to the regions handling emotional processing, such as the visual cortex. In 2015, neural synchronization between θ waves and γ activity was linked to emotional control over the anterior prefrontal cortex [6]. In 2016, the higher-frequency activities (β/γ-band) in the frontal lobe were found to be significantly correlated with valence [7]. In 2019, the prefrontal area revealed stronger β/γ-band power under negative emotions than under positive emotions, while both the positive and neutral states presented higher α responses at parietal and occipital sites [8].

These reports indicated that the prefrontal/frontal cortex served as a critical lobe in emotional processing in particular. Therefore, the present study emphasized the cross-couplings in the six montages mainly over the frontal/prefrontal area.

Several studies have focused on quantitative features, such as power spectral density [9], coherence [10], and differential asymmetry [11] of EEG recordings, to characterize emotional processing. However, the mechanism of mutual interactions between EEG rhythms under different emotional expressions lacks full exploration, which reflects the characteristics of neuromodulation during emotional processing. Cross-frequency coupling (CFC) measured the interactions between rhythms with distinct scales and spatial montages while serving as a critical formation for both local calculation and global communication [12], [13]. Phase-amplitude coupling (PAC), which is defined as the capacity of a lower-frequency phase to modulate its higher-frequency amplitude, attracts the most attention. Low-frequency oscillations control long-range synchronization, and high-frequency power is linked to local computation [14]. Since its proposal, PAC has become a popular method for a variety of studies, such as decision-making [15], gait disturbance [16], and spasticity [17]. The mutual correlation and the nested nature of brain activities across different populated levels and time scales indicate that PAC is a potential feature for emotion.

Precisely extracting phase and amplitude modulations of oscillatory input is an important step in guaranteeing reliable PACs. A traditional sinusoidal basis function fails to adapt nonstationary oscillation because of a loss of temporal information. A set of wavelet basis functions was then introduced to address this limitation [18]. The corresponding wavelet decompositions present a proper time-frequency resolution than that of the Fourier transform, i.e., a higher frequency range presents finer temporal and lower frequency resolution, and vice versa [19]. However, its linear nature may result in harmonics. In the last decade, the implemented use of empirical mode decomposition (EMD) [20] and its improved versions such as ensemble EMD (EEMD), have shown themselves to be adaptive to nonlinear and nonstationary complex systems. Briefly, a set of intrinsic mode functions (IMFs) free of riding waves are generated through a sifting process with their local mean curves close to zero at any point, guaranteeing reliable instantaneous frequencies in IMFs. In 2014, Pittman-Polletta et al. [21] integrated EMD into PAC, extracting broadband components accounting for the length limitation and oscillatory nonstationarity/nonlinearity in calculating PAC. Since then, EMD has been applied more to studies with CFCs [12]. Nevertheless, the mode-mixing problem of EMD is inevitable, meanwhile, its interpolation process that generates the envelope is susceptible to sampling. On the other side, the iterative filter (IF) that used a priori chosen "filter function" to derive the moving average of each component is an alternative to calculate the averaged envelope in the EMD sifting process, with given mathematical criteria and convergence [22]. However, spike pulses in the signal could substantially affect signal decomposition and induce spurious coupling. Motivated by the demands for relative narrowband IMFs and robust decomposition, the variational mode decomposition (VMD) method was proposed [23] by generating an ensemble of modes that optimally reconstruct input, wherein each mode is band-limited around a center frequency. Intrinsically, VMD equals a generalization of the Wiener filter, a common denoising tool, resembling the application of a set of filters to multiple adaptive frequency bands and is thus relatively robust to noise contamination. In this work, a novel method called variational phase-amplitude coupling (VPAC), with the creative use of VMD, is proposed for investigating emotional dynamics with EEGs.

The remainder of this study is organized as follows: In Section II, we present the materials and the proposed method. In Section III, we give the simulated results and EEG emotion modulation results based on VPAC. A discussion is presented in Section IV. Finally, we conclude the paper in Section V.

II. Methods

A. Materials and Preprocessing

The standard EEG database DREAMER for emotion recognition is included in this work. The details of the experiments are stated in [25] with the acquisition and publication of the anonymized data approved by the University of the West of Scotland University Ethics Committee [25]. Fourteen EEG unipolar electrodes of 23 healthy subjects were collected. The sampling rate of EEGs was 128 Hz. The experiment consisted of eighteen trials of movie clips corresponding to nine emotions, i.e., three positive emotions (amusement, excitement, and happiness), one neutral emotion (calmness), and five negative emotions (anger, disgust, fear, sadness, and surprise). The trial length varied from 65 to 393 s. To ensure sufficient elicitation of respective emotions, only the recordings captured in the last 60 s of each film clip were used for the additional analyses. The experiment started with a neutral film clip to facilitate the subject's return to a neutral emotional state and establish the baseline recording. After watching a film clip, the self-assessment questionnaires were used to acquire subjective assessments of their emotions.

We emphasized the six EEG channels (AF3-AF4, F3-F4, and FC5-FC6), mainly in the frontal area, in terms of their tight linkage to emotional responses [26]. Since the average values across subjects in terms of valences for two film clips eliciting a surprised reaction, one represents a positive valence and the other represents a negative valence, we excluded these two trials and disregarded the emotion of surprise. The baseline per segmented EEG was adjusted to zero. A notch filter at 50 Hz followed by a high-pass filter at 0.5 Hz cutoff frequency was applied to remove artifacts. Principal component analysis and fast independent component analysis were used to estimate the independent components of EEGs to eliminate contamination from eye movements, eye blinks, and cardiac rhythms.

B. Variational Mode Decomposition

VMD is a nonrecursive signal decomposition method essentially based on the Wiener filter, Hilbert transform, and heterodyne demodulation. A real-valued input signal $f(t)$ can be decomposed into K discrete subsignals (modes), u_k ($k = 1, 2, \ldots, K$), by VMD. Unlike EEMD, each mode u_k is formulated as

an amplitude-modulated-frequency-modulated (AM-FM) signal with confined bandwidth compacting around a center frequency ω_k, which is determined through the decomposition.

To assess the bandwidth of a mode, the following schemes were proposed. First, the analytic form of a mode was computed through the Hilbert transform to obtain a unilateral frequency spectrum. Next, the frequency spectrum of a mode was shifted to a "baseband" by multiplying the input with an exponential term so that the decompositions are tuned to the respective estimated center frequencies. Last, the bandwidth of each mode was estimated by calculating the L^2-norm of the shifted signal. The resulting constrained variational optimization problem can be formulated as

$$\min_{\{u_k\},\{\omega_k\}} \left\{ \sum_k \left\| \partial_t \left[\left(\delta(t) + \frac{j}{\pi t} \right) * u_k(t) \right] e^{-j\omega_k t} \right\|_2^2 \right\} \times s.t. \sum_k u_k = f \tag{1}$$

where $\{u_k\} := \{u_1, \ldots, u_K\}$ denotes the set of all decomposed modes, $\{\omega_k\} := \{\omega_1, \ldots, \omega_K\}$ represents the set of corresponding center frequencies, $\delta(t)$ is the Dirichlet function, and $*$ stands for the convolution operator symbol.

To solve the constrained optimization problem and obtain the optimal mode, a quadratic penalty factor α and a Lagrangian multiplier λ were introduced, of which α guarantees the reconstruction precision of a signal in the presence of strong noise interference, while λ renders the problem unconstrained. The resulting augmented Lagrangian function is stated as

$$\begin{aligned} &L(\{u_k\}, \{\omega_k\}, \lambda) \\ &:= \alpha \sum_k \left\| \partial_t \left[\left(\delta(t) + \frac{j}{\pi t} \right) * u_k(t) \right] e^{-j\omega_k t} \right\|_2^2 \\ &\quad + \left\| f(t) - \sum_k u_k(t) \right\|_2^2 + \left\langle \lambda(t), f(t) - \sum_k u_k(t) \right\rangle \end{aligned} \tag{2}$$

The saddle point of the augmented Lagrangian function is next accessed with the alternating direction method of multipliers, and the optimal solution is obtained. The complete algorithm of VMD in the time domain is illustrated in Fig. 1, whereas Parseval/Plancherel Fourier isometry is the key to solve the ill-posed inverse problem in the spectral domain under the L^2-norm [23].

The decomposed mode functions $\{u_k, k = 1, \ldots, K\}$ obtained through VMD are quasi-orthogonal and sorted in descending order by frequencies. The instantaneous amplitudes/envelopes $A_k(t)$ and phases $\varphi_k(t)$ of the corresponding mode functions $\{u_k\}$ are calculated by the Hilbert transform $H\{\cdot\}$. The analytic form $\psi_k(t)$ of $u_k(t)$ can be formulated as a complex function:

$$\psi_k(t) = u_k(t) + jHu_k(t) = A_k(t)e^{j\varphi_k(t)} \tag{3}$$

The instantaneous phase $\varphi_k(t)$ of the mode $u_k(t)$ is given as

$$\varphi_k(t) = \arctan \frac{Hu_k(t)}{u_k(t)} \tag{4}$$

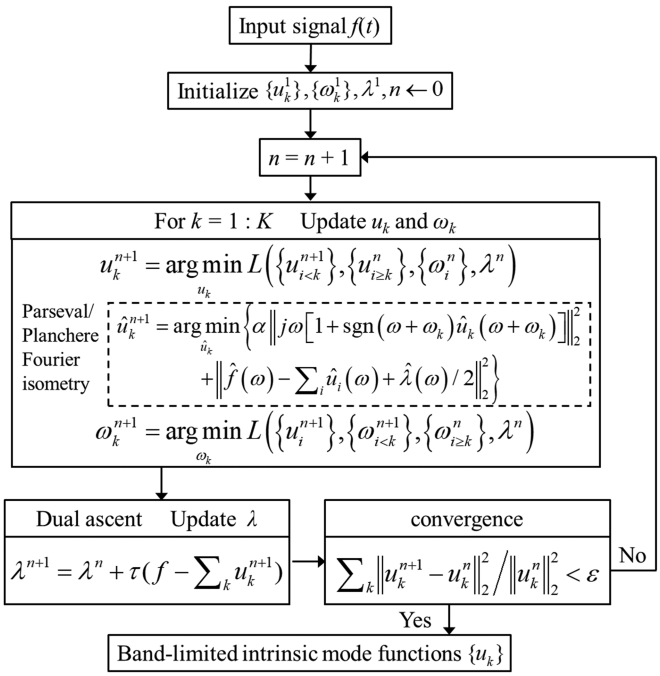

Fig. 1. Flow chart of alternate direction method of multipliers for VMD, where τ denotes time-step of the dual ascent. ε represents the tolerance of convergence criterion.

whereas its instantaneous amplitude is written as

$$A_k(t) = \sqrt{u_k(t)^2 + Hu_k(t)^2} \tag{5}$$

C. Modulation Index

Among the quantification methods for cross-frequency coupling, the modulation index (MI) [27] is well recognized as an ideal quantity for assessing the intensity of PAC. MI, an adaptation of the Kullback–Leibler (KL) distance, measures the degree to which a distribution of the high-frequency amplitude locked on the low-frequency phase deviates from a uniform distribution. The algorithm for calculating MI is illustrated as follows. First, the phase and amplitude time series of $u_k(t)$ were obtained using the Hilbert transform by (4) and (5). Next, all phases from 0 to 2π were divided into N bins ($N = 20$). The average high-frequency amplitudes were calculated over the low-frequency phase bins through all samples of a pair of decompositions and then such a phase-amplitude distribution was normalized, referring to the proportion of high-frequency amplitude over each phase bin. The KL distance was formulated as $D_{KL}(P,U) = \log N - H(P)$, where U represents the uniform distribution, while $H(P)$ stands for the Shannon entropy of the distribution P, defined as $H(P) = -\sum_{j=1}^{N} P(j)\log[P(j)]$. Note further that log$N$ is the maximal possible entropy value, implying a uniform distribution (i.e., $P(j) = 1/N$ for all bins j). Finally, a quantity termed MI was obtained by dividing the KL distance of the observed amplitude distribution P from the

uniform distribution U by log$N$, i.e.,

$$\mathrm{MI} = \frac{D_{KL}(P,U)}{\log N} \tag{6}$$

The MI approaches zero, while amplitudes over all possible phase bins are relatively uniform; in contrast, the MI equals one, while the distribution follows the Bernoulli distribution.

D. Cycle-by-Cycle Frequency

The VMD method extracted components with slowly varying and positive envelopes. The procedure of shifting the spectrum of the modes to the "baseband" refers to adjusting the decomposition to the respective estimated center frequency, which could be independent of local extrema and their interpolation for envelope forming like EMD. Its robustness to noise contamination minimized the risk of spurious coupling caused by complex and intermittent noise from neurophysiological time series. Unlike EMD, which can fail to discriminate components that are close in frequencies, the narrow-band property of VMD enables it to separate precisely so which improves both the frequency resolution and accuracy of PAC. However, the direct use of VMD with PAC algorithm can result in a lower frequency resolution due to the variable frequencies of decompositions. Therefore, the VPACs were designed to redistribute across a scattering-frequency plot as per the cycle-by-cycle frequencies of each IMF pair as follows.

First, we unfolded the phase time series $\varphi_k(t)$. Next, the conversions between periods were defined as the time points at which the expansion phase time series spans a 2π integer increment. The cycle-based frequency time series $f(u,v)$ beginning from a time point u and ending at a time point v was then calculated by the following formula:

$$f(u,v) = \left(\frac{f_s}{v-u}\right) \cdot \left(\frac{\varphi_k(v) - \varphi_k(u)}{2\pi}\right) \mathrm{Hz}$$
$$F_k(s) = f(u,v), u < s < v \tag{7}$$

where f_s is the sampling frequency of the input signal $f(t)$. We set $F_k(s) = f(u,v)$ for all s between u and v. Hence, the cycle-based frequency time series can be a secant approximation to that of the instantaneous value, which is the derivative of the instantaneous phase time series. Unlike the instantaneous frequency, which is sensitive to sharp changes in pattern, the proposed cycle-by-cycle frequency framework is insusceptible to such factors. Of note, compared to a smoothed instantaneous frequency series, the proposed framework enabled us to focus on the interwave modulation per se [21], [24].

E. Surrogate Testing

To match the cycle-by-cycle framework, a "block shuffle" procedure was implemented in the cycles (i.e., blocks) of the phase and amplitude modulations, followed by random permutations of these blocks [21]. To determine the empirical distribution for the i^{th} amplitude-given component and the j^{th} phase-given component, the cycles of $A_i(t)$ and $\varphi_j(t)$ were shuffled as follows. For each $A_i(t)$ and $\varphi_j(t)$, all cycles were assigned an index (of note, cycles across time series are independent); then, the cycle indices were randomly and sufficiently switched to yield a nearly random permutation of cycles [28]. Finally, the cycles (probably unequal length) were concatenated according to the randomly permuted cycle indices. In the resulting shuffled phase and amplitude time series $\hat{\varphi}_j(t)$ and $\hat{A}_i(t)$, the temporal relationship between high-frequency amplitudes and low-frequency phases is disordered, but the phase and amplitude profiles of individual cycles remain intact. The MI of $\hat{\varphi}_i(t)$ and $\hat{A}_i(t)$ thus is unable to reflect phase-amplitude coupling, which is the interaction of simultaneously occurring phases and amplitudes. In this work, we repeated the "block shuffle" process 100 times for each pair of oscillatory components. The mean and standard deviation of the MI empirical distribution obtained were used to determine the z *score* of the observed MI for each pair of components. Measurements that failed to exceed a significance level of $\alpha = 0.05$ were ignored.

F. Visualization of the VPAC Frequency Plane

A phase-amplitude comodulogram is a useful tool for exhibiting the strength of couplings between multiple frequency band pairs simultaneously. To secure high-frequency resolution, we assigned an MI value associated with a pair of components to a plane as per the corresponding cycled frequencies of all sample pairs; precisely, a value representing the significant MI was assigned to the corresponding frequency coordinates. After repeating the aforementioned process to all pairs of components, the redistributed MIs were averaged over a predetermined rectangle patch of phase-amplitude frequency space. In this work, a rectangle patch of 0.2 Hz × 0.4 Hz (phase frequency × amplitude frequency) was applied in the analysis of the EEG dataset, of which the former ranged between 1.9 Hz and 30.3 Hz, whereas the latter spanned from 6 Hz to 60 Hz. For the simulation, the low-frequency bin was 0.4 Hz, while the high-frequency band was set as four Hz and two Hz, corresponding to nonlinear and nonstationary sets, respectively. Fig. 2 shows a schematic diagram of the proposed VPAC algorithm.

G. Phase-Locking Value

The phase-locking value (PLV), as an index measuring consistency in phase alignment across a pair of time series, is defined as

$$\mathrm{PLV} = \frac{1}{N}\left|\sum_{i=1}^{N} \exp\left[i\left(\varphi_{f_p} - \varphi_{A_{f_A}}\right)\right]\right| \tag{8}$$

where N represents the number of time points, φ_{fp} stands for the phase time series, and φ_{AfA} is the phase angle of the Hilbert envelope. Briefly, the phase-angle differences between the envelope of amplitude-given oscillation and the phase-given wave are calculated as an alternative to the standard PAC computation. Visually, the phase-angle differences of all sample pairs are scattered in a polar plane, wherein the angle stands for the respective phase angle difference, while the mean vectors of all samples from the center define PLV. A constant phase lag across all samples implies strong PAC, referring to all vectors in a polar

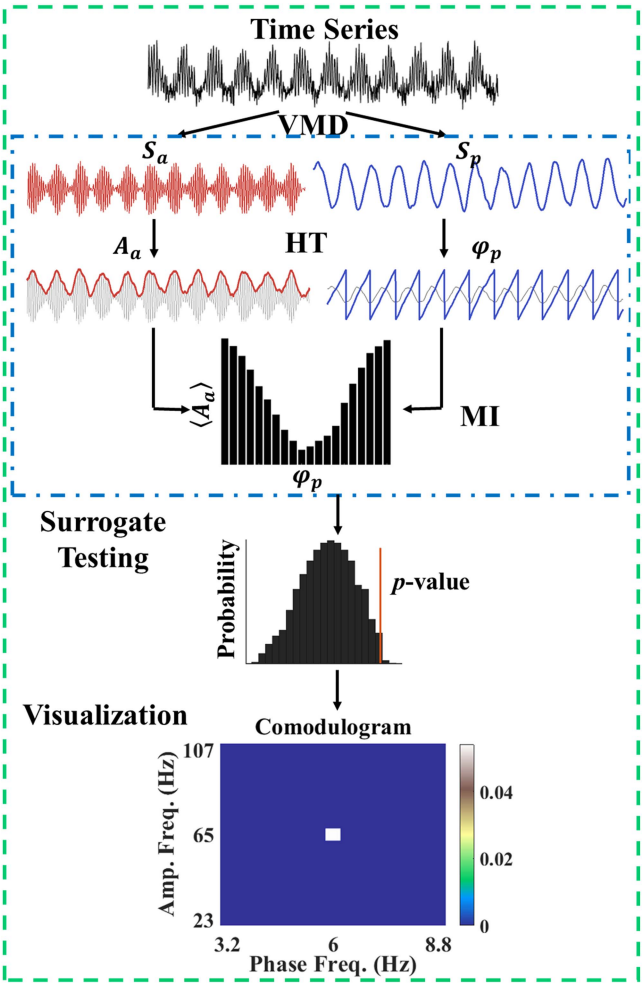

Fig. 2. Schematic diagram of VPAC algorithm. Firstly, a synthetic signal with nonstationary characteristics which resemble EEG is illustrated. Then, the phase-given S_p and amplitude-given S_A modes are extracted by VMD to target the contributing nonstationary modes. Next, the instantaneous envelopes A_a and phases φ_p of the corresponding modes are calculated by hilbert transform with MI used to measure coupling strength. Then, surrogate data are generated to test the significance of MI with sustained temporal structure. Lastly, a comodulogram is used to visualize multi-frequency coupling strength.

plane with the same direction (i.e., phase-locked; PLV = one); conversely, the vectors of all samples randomly scatter around the polar plane if the phase lags are variable (i.e., completely desynchronized; PLV = zero).

H. Statistical Analysis

A general linear mixed model (GLMM) was applied to test the ability of VPAC to distinguish emotions under rough/specific classifications and EEG regions/channels on the given pairwise frequencies, of which the subjects were set as a random factor. Two-tailed *p values* less than 0.05 were regarded as statistically significant for the test. The Shapiro–Wilk W test was used to assess normality. Student's *t test* was adopted for multiple comparisons to test all possible pairwise differences of means. The physiological data were analyzed in MATLAB (MathWorks, Natick, MA). All statistical analyses were conducted using JMP, a Business Unit of SAS.

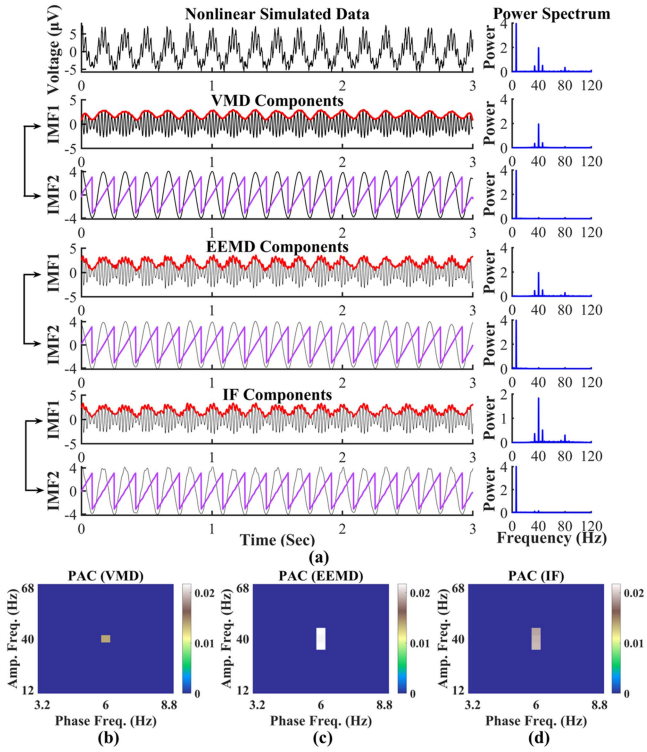

Fig. 3. Nonlinear simulated data were designed to verify the performance of the proposed method. (a) Nonlinear signal with a degree of nonlinearity equal to two. The performance using (b) VMD, (c) EEMD, and (d) IF are shown.

III. Results

A. Simulations

To verify the performance of the proposed method, we applied VPAC to nonlinear and nonstationary synthetic signals against PAC decomposed with EEMD and IF. The simulated signal $S(t)$ was designed by a phase-given oscillation $S_p(t)$ and an amplitude-given oscillation $S_a(t)$ with a sampling rate of 600 Hz and a data length of 10 seconds. The simulated nonlinear oscillations were constructed by splicing two half-cycled patterns of sinusoidal functions with the same amplitude but not necessarily the same periods [29]. The degree of nonlinearity was defined as the ratio of the periods of the two sine functions.

The analyzed nonlinear signal was designed as a 6-Hz phase modulating 40-Hz amplitude, of which the degree of nonlinearity equaled two [30]. VMD, EEMD, and IF were used for signal decomposition. Fig. 3(a) shows the time series of the simulated nonlinear signal, VMD decompositions, EEMD decompositions, IF decompositions, and their respective power spectra. Considering that two main components are presented in the uppermost right panel of Fig. 3(a), we set K = two in the VMD decomposition. Compared to the EEMD and IF results, VMD demonstrated fewer ripples in high-frequency mode. Although centralized 6 Hz-to-40 Hz PAC using VMD, EEMD, and IF

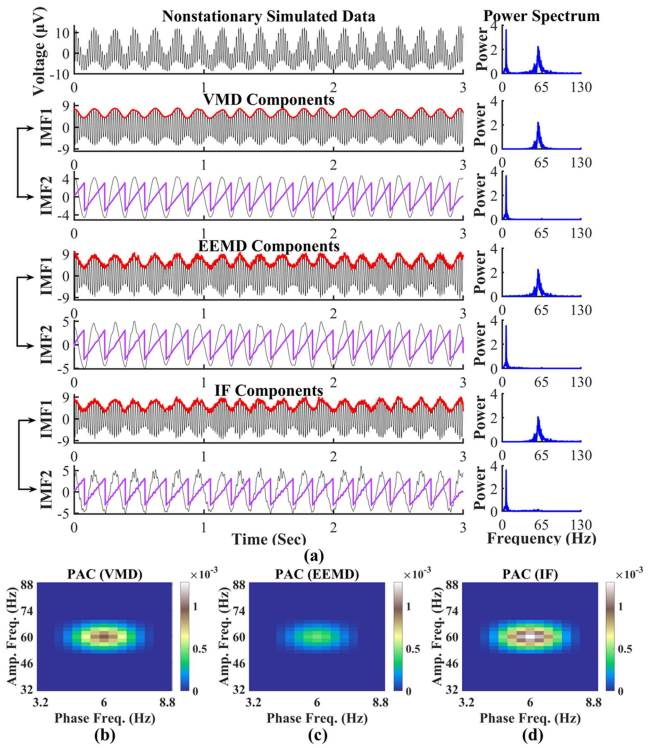

Fig. 4. Nonstationary simulated data were designed to verify the performance of the proposed method. (a) Nonstationary simulated signal with varying low-frequency phases and high-frequency amplitudes. The performance of PAC is shown with a comparison between (b) VMD, (c) EEMD, and (d) IF.

are both presented in Fig. 3(b), (c), and (d), the PAC result of EEMD and IF showed slight leakage in the identification of amplitude, resulting in spurious phase-amplitude coupling at 6-36 and 6-44 Hz. As expected, VMD exhibited robustness to nonlinear couplings.

For the nonstationary cross-couplings, the simulated signal was independently constructed by the randomly determined cycle-by-cycle frequencies of both phase and amplitude modulations. Here, the phase was set between five and eight Hz, and the amplitude varied from 55 to 65 Hz. Likewise, two main components at approximately six Hz and 60 Hz appeared in the amplitude spectrum shown in Fig. 4(a) (top-down panels: simulated nonstationary signal and the corresponding VMD, EEMD, and IF decompositions, respectively). Thus, K was also set as two for VPAC. The two VMD modes showed favorable separation compared to the designs over the time domain. Ideally, elliptical coupling centered at approximately 6-60 Hz was presented by the VPAC comodulogram (Fig. 4(b)). On the other hand, the coupling-strength distribution of the EEMD-PAC of approximately 6-60 Hz frequency pairs presented lower gradients, thus less precisely allocating the target frequencies of interest in couplings (Fig. 4(c)). Meanwhile, IF performed more ripples in low-frequency mode (time series on the bottom left panel of Fig. 4(a)). The simulation results revealed that the proposed VPAC can be a promising method for quantifying phase-amplitude coupling for nonlinear and nonstationary signals, such as EEGs compared to EEMD/IF-based PAC.

B. VPAC Results Under Emotional Processing

In this subsection, the proposed VPAC was applied to explore the phase-amplitude coupling properties of physiological responses elicited by emotions. The EEGs accessed on the frontal lobe are mainly discussed. Considering that the number of modes in VMD (i.e., K values) can be set in advance, the power spectra of the analyzed EEGs were carefully inspected, and the robustness of each decomposition with K ranging from three to eight was compared. Of these, the estimated center frequency converged relatively precisely to the EEG frequencies of interest when K equaled six. The effective modes were neither discarded as noise artifacts nor split patterns, and were further used for the emotional cross-coupling analyses. The center frequencies of each mode were initialized uniformly due to its wide spread of frequencies [31]. In addition, modes with an averaged cycle-by-cycle frequency lower than three Hz were excluded to eliminate unrelated PACs to emotional processing [25].

Fig. 5(a) demonstrates the preprocessed EEG recording of one subject in the DREAMER dataset with the amplitude spectrum set aside. Clearly, the energy was mainly confined to lower than 50 Hz. The decomposed modes with an average cycle-by-cycle frequency greater than three Hz and their respective amplitude spectra are shown in Fig. 5(b). The corresponding center frequencies of each mode were located at 4, 11, 18, 25, and 33 Hz, respectively, with clear spectral partitioning. As expected, the mode mixing or splitting phenomenon was greatly improved compared to that of EEMD. Following this, a phase-amplitude comodulogram result is exhibited in Fig. 5(c). Interestingly, block-distributed phase-amplitude frequency pairs are scattered around the upper triangle of this graph, indicating that the driven phase-frequency bands were dispersed in small frequency ranges rather than in a broad frequency band. To obtain the specific frequency bands of PAC related to emotion types, we went through the comodulogram results of all subjects and channels and divided the scattered frequency pairs into 11 parts (Table SI). However, not all 11 frequency pairs showed significant differences in various emotional comparisons. Our results revealed that the mean MIs of Freqs. 1, 5, 9, 10, and 11 under different emotions were statistically significant. Therefore, these five frequency pairs are mainly discussed below.

In observing an overall phase-amplitude coupling characteristic of different emotions in various brain regions, topoplots showing average MIs under the five frequency pairs were meticulously drawn. For each frequency pair, two emotions with the greatest significant difference were selected, and the results are shown in Fig. 6. Calmness and amusement were the two representative emotions selected from the set of Freq. 1. In this set, the α amplitudes were modulated by the δ/θ phases (Fig. 6(a)). We found that the δ/θ-α PAC for calmness was obviously stronger in the AF region overall than that for the emotion of amusement, as well as for the remaining six emotions, especially in the AF4 channel (see the leftmost panel

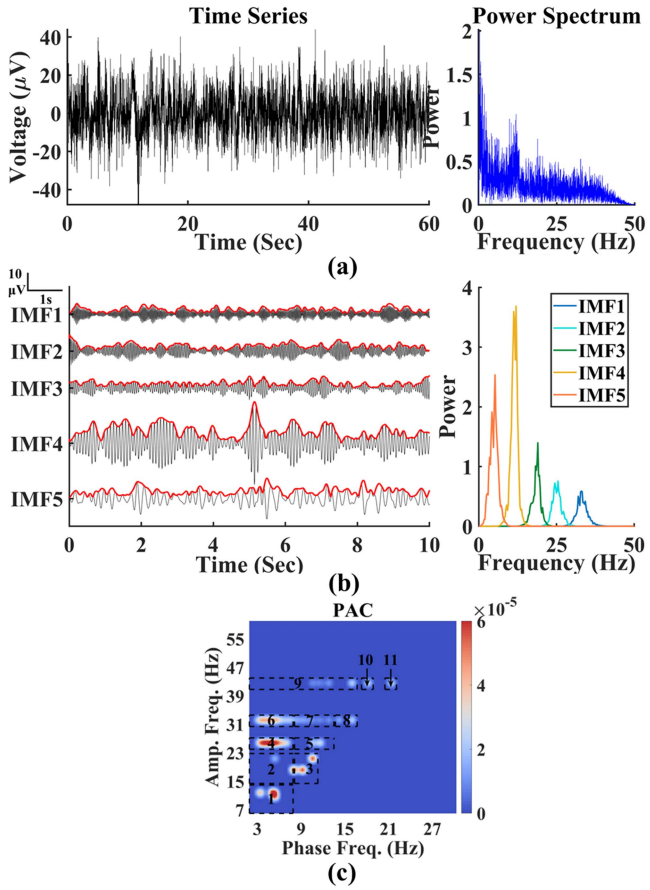

Fig. 5. The preprocessed EEG plot (a) and its corresponding decompositions (b) using the VMD of one subject in the DREAMER dataset with respective amplitude spectrum set aside. (c) The phase-amplitude comodulogram of this subject, and the divided 11 frequency pairs shown in the figure.

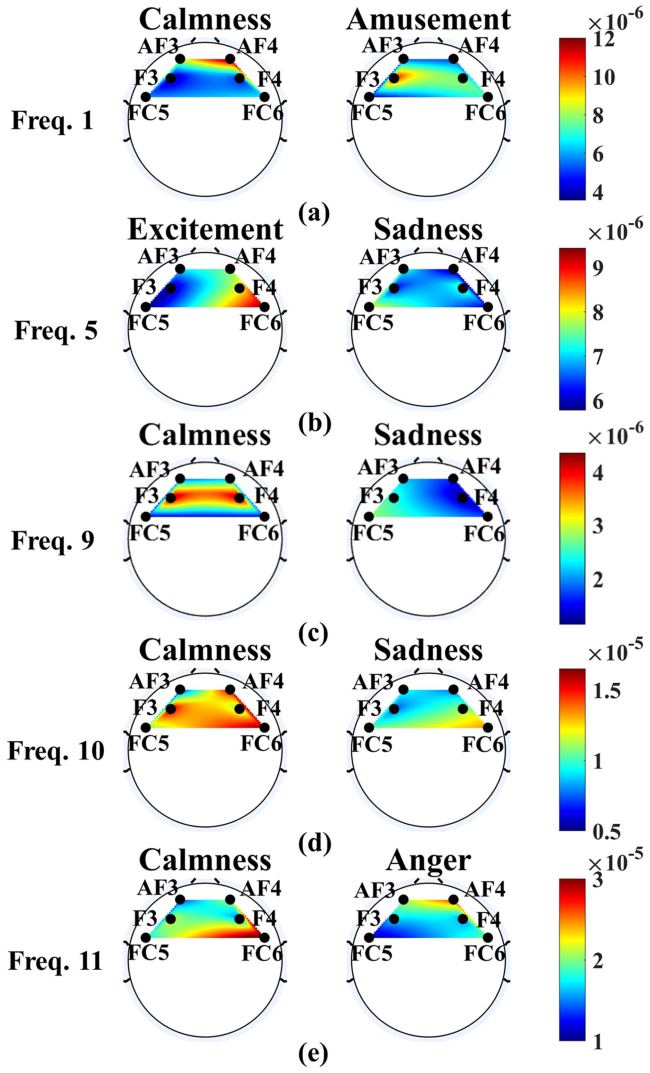

Fig. 6. Topoplots of the mean MIs for the two emotions in five frequency pairs with statistically significant MIs.

of Fig. S1(b), $p = 0.0023$). However, for the same frequency, pairwise, of PACs in the frontal region, amusement generally displayed a stronger coupling strength than calmness, particularly in the F3 channel (middle panel of Fig. S1(b), $p = 0.0043$). The coupling strength of neutral emotional state was weaker than that of negative or positive emotion, while the frequency interval rose to that of Freq. 5. Interestingly, for excitement, clear asymmetric frontal PAC emerged, mainly greater in the right frontal region (Fig. 6(b)). At Freqs. 9, 10, and 11, the modulated amplitude-frequency was fixed at 41-44.2 Hz, with an increase in the phase-given frequencies, and the overall phase-amplitude coupling strength increased by nearly an order of magnitude (from 4×10^{-6} to 3×10^{-5}). On the other hand, for the neutral state, with an increase of phase-given frequencies, the coupling strength increased, as well as the modulation region transited from the anterior-frontal region to the frontal-central region (left panels from Fig. 6(c) to (e).

Next, we chose the PAC in Freq. 11 with the greatest coupling strength relative to other frequency pairs as a representative to use to discuss the expression of different emotions in various brain regions. The lack of distinction between the left and right cerebral channels is shown in Fig. 7. The specific phase and amplitude-frequency band of Freq. 11 are shown in Fig. 7(a), and the brain map of the three sets of montages is presented in Fig. 7(b). An ANOVA with brain region and rough emotional state as factors revealed only a main effect of emotion type ($p = 0.0387$) (Table I). Post hoc analysis revealed that, in the FC region, the neutral emotional state showed a significantly stronger high β-γ PAC than the positive/negative emotional state (see the rightmost panel in Fig. 7(c); $p = 0.0055$). The calmness emotion still exhibited a significantly stronger high β-γ PAC in the FC region than the other seven emotions, as expected (see the rightmost panel in Fig. 7(d); $p = 0.0056$). An ANOVA with brain region and specific emotion as factors revealed only a main effect of emotion ($p = 0.0501$) (Table I). Post hoc analysis demonstrated that after emotional subdivision, the anterior frontal region also showed significant differences, of which the high β-γ PAC of anger was significantly stronger than that of the other seven emotions (the leftmost panel in Fig. 7(d); $p = 0.0020$), and the high β-γ PAC of disgust was the weakest ($p = 0.0646$).

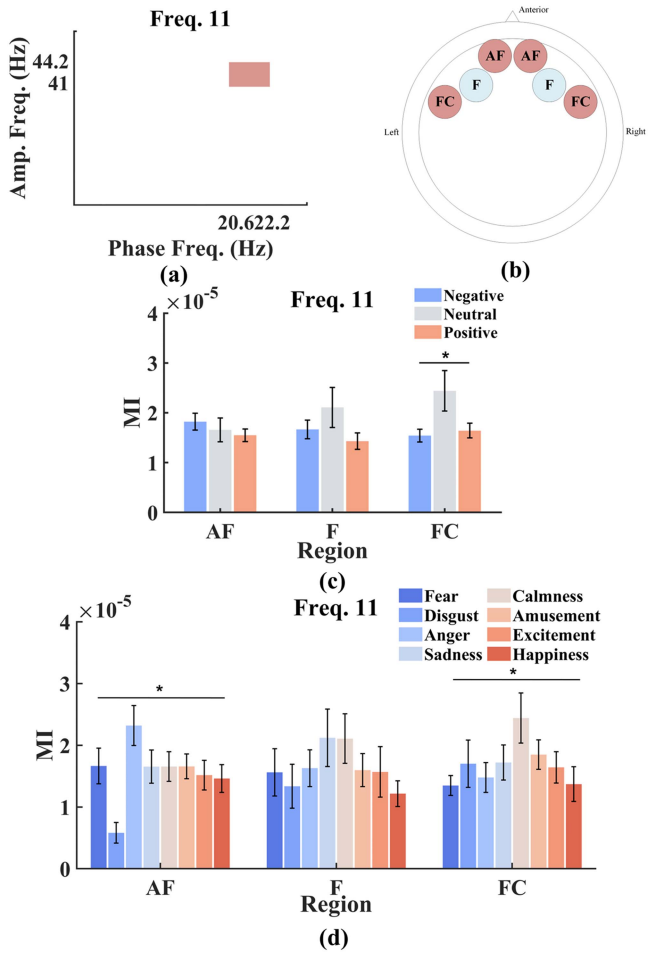

Fig. 7. Comparisons of the mean MIs among different emotions with frequency pair 11 in three different brain regions. (a) The frequency coordinates of freq. pair 11 are shown. (b) The regions with statistical signficance among emotions are marked as pink. Significance tests on MIs among (c) three rough emotional states, or (d) eight specific emotions are tested. $*$ means $p < 0.05$.

TABLE I

THE MEAN MIS OF FREQUENCY PAIR 11. ALL POSSIBLE PAIRWISE COMBINATIONS OF THE FOUR FACTORS INCLUDE BRAIN REGION (THREE LEVELS: AF, F, AND FC), EMOTIONAL STATE (THREE LEVELS: POSITIVE, NEUTRAL, AND NEGATIVE), CHANNEL (SIX LEVELS: AF3, AF4, F3, F4, FC5, AND FC6), AND SPECIFIC EMOTION (EIGHT LEVELS: AMUSEMENT, EXCITEMENT, HAPPINESS, CALMNESS, ANGER, DISGUST, FEAR, AND SADNESS). SIGNIFICANT *P VALUES* AND THOSE SHOWING TRENDS ARE EMBOLDENED

Factor	DF	MS	F value	P value
Region	2	2.28e-10	0.6938	0.5002
State	2	1.08e-09	3.2751	**0.0387**
Region*State	4	9.29e-10	1.4152	0.2279
No distinction between left and right brain, emotional state classification				

Factor	DF	MS	F value	P value
Region	2	5.52e-11	0.3362	0.7147
Emotion	7	3.33e-10	2.0301	**0.0501**
Region* Emotion	14	1.64e-10	0.9974	0.4548
No distinction between left and right brain, specific emotion classification				

Factor	DF	MS	F value	P value
Channel	5	6.68e-10	4.2492	**0.0009**
State	2	3.40e-10	2.1651	0.1160
Channel*State	10	1.99e-10	1.2647	0.2481
Distinction between left and right brain, emotional state classification				

Factor	DF	MS	F value	P value
Channel	5	6.91e-10	4.4622	**0.0006**
Emotion	7	1.96e-10	1.2689	0.1160
Channel*Emotion	35	1.93e-10	1.2	0.2481
Distinction between left and right brain, specific emotion classification				

A finer analysis of PACs in Freq. 11 for six different brain electrodes is depicted in Fig. 8. The specific phase and amplitude-frequency band of Freq. 11 are shown in Fig. 8(a), and the brain map of the six channels is presented in Fig. 8(b). An ANOVA with channel and rough emotional state as factors revealed a significant effect of the channel ($p = 0.0009$) (Table I). In the post hoc test, a stronger high β-γ PAC under neutral emotion was mainly revealed in the FC6 channel ($p = 0.0139$). However, a statistically stronger high β-γ PAC under neutral emotion emerged in the F3 channel ($p = 0.0105$), which was opposite to the performance of the F4 channel, although no significant difference was shown (Fig. 8(c)). This asymmetric phenomenon led to a comparable level of high β-γ PAC in the frontal region among the three emotional states (middle panel in Fig. 7(c)). More specifically, in the emotional subdivision, an ANOVA with channel and specific emotion as factors revealed a significant effect of the channel ($p = 0.0006$) (Table I). In the post hoc test, the high β-γ PAC under neutral emotion (calmness) was lower than that of the negative ones, especially anger and sadness, in the anterior frontal region, gradually increased in the F3 region, and was the highest in the frontal-central region (Fig. 8(d)). Unlike the rest of the negative emotions, the disgust emotion presented a weak high β-γ PAC in the channels of the anterior frontal, which neutralized the strong high β-γ PACs under the other negative emotions. The coupling strength of the disgust emotion gradually increased in the frontal region and reached its strongest in the right frontal-central region (Fig. 8(d)).

The VPAC results of the four other frequency pairs are provided in the supplementary material. Significant PACs under the neutral emotional state gradually shifted from the anterior to the central area of the brain with an increase in the driving phase, under the premise of carrying γ-band amplitude modulation, of which the coupling strength of the neutral emotional state was stronger than that of positive and negative emotions in the frontal and frontal-central areas (Fig. 7). Conversely, in the frontal and frontal-central areas, if the modulated amplitude had either α or β rhythm, the PACs under positive or negative emotional states would be stronger than that under the neutral emotional state (result not shown).

Moreover, we explored the phase-angle differences and PLVs for all frequency pairs with significant differences in VPAC among emotions. Representative results with the strongest VPAC in the respective channels are shown in Fig. 9. We divided the 60-s data into 5-s nonoverlapping segments, from which a stable emotional state can be indicated when deriving the phase-locking value. The averaged cycle-by-cycle frequency of each IMF was used as a criterion to identify whether an IMF was either a high- or low-frequency component. The cross-subject scatter

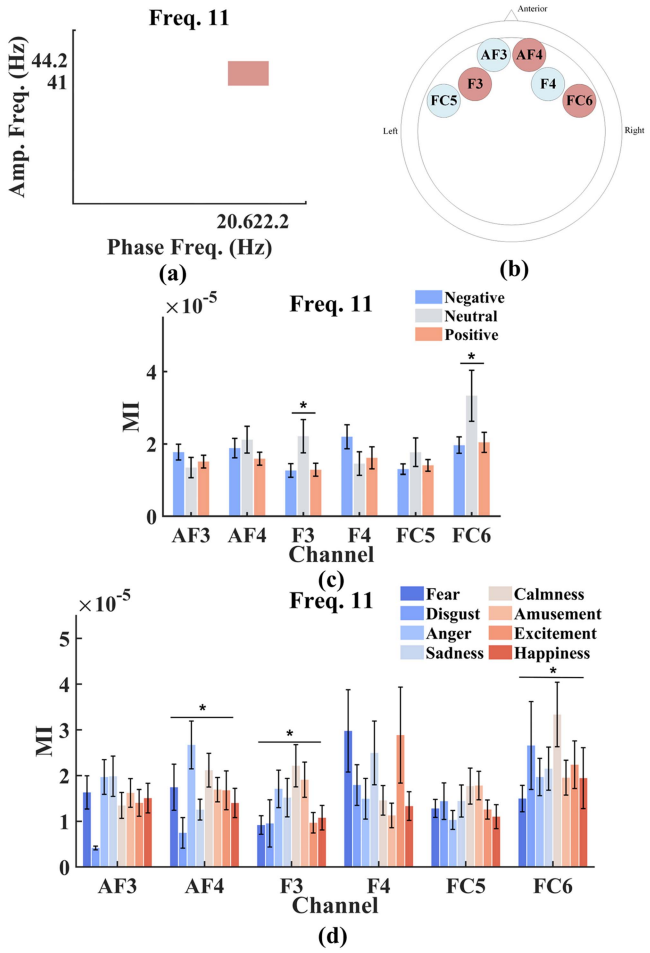

Fig. 8. Comparisons of the mean MIs among different emotions with frequency pair 11 in the six different channels. (a) The frequency coordinates of freq. pair 11 are shown. (b) The channels with statistical significance among emotions are marked as pink. Significance tests on MIs among (c) three rough emotional states or (d) eight specific emotions are tested. $*$ means $p < 0.05$.

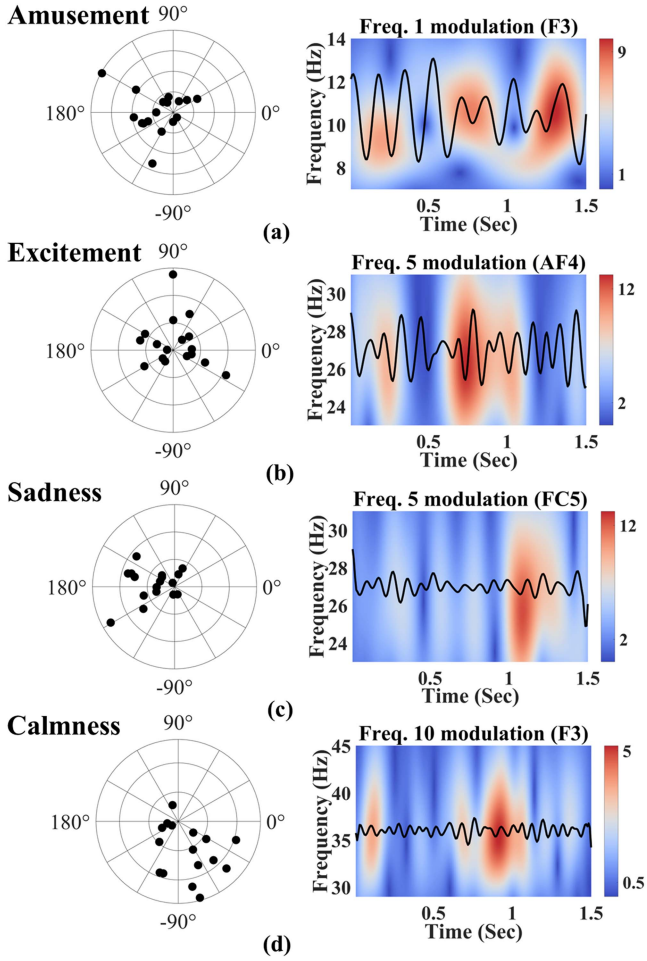

Fig. 9. Phase difference scatters and the respective time-frequency plots of (a) amusement, (b) excitement, (c) sadness, and (d) calmness. The vectors in the left panels equal to values of PLV and the time-frequency plots and black lines represent higher and lower frequency IMF in the right panels, respectively.

diagram in polar coordinates shows the distribution of averaged phase differences between the specific frequency pairs (left panels in Fig. 9). On the other hand, the right panels of Fig. 9 present the phase shift across different emotional processing, in which the time-frequency spectrograms belong to the high-frequency oscillations, while the black traces denote the low-frequency waves. Several leading phase shifts contributed to the coupling of positive emotion; in contrast, negative/neutral emotion exhibited a relatively concentrated distribution. Fig. 9(a) shows that the peak of the α amplitude lagged behind that of the δ/θ phase, clustering approximately 150° and -120° relatively consistently for amusement in F3. The phase shift between the α phase and the phase of the β amplitude (24.2-27.2 Hz) was approximately 90° and -30° in AF4 for excitement (Fig. 9(b)), whereas the local maximum of the β-band amplitude (24.2-27.2 Hz) laid on the near trough of the α phase in the FC5 for sadness in Fig. 9(c), which implied the different results of VPAC between positive and negative emotions was not only reflected in different brain regions but also expressed different phase shifts. Fig. 9(d) depicted the γ power peak that emerged at the ascending phase of β in the F3 for calmness.

IV. Discussion

In this work, we mainly emphasized the mechanism of cross-frequency entangling oscillations of EEGs under different emotional expressions.

As per our findings, the PACs given γ amplitude seems to contribute more to the emotion processing pathway, either rough emotional state or specific emotion, which is consistent with the hypothesis that rapid cortical neural activities associate with consciousness [32]. γ oscillation is also generally considered a typical representation of the integration of distributed neural processes into high-order cognitive functions, such as emotional processing [33]. Our results showed that the amplitude of γ-band oscillation was modulated by multiple low-frequency phases (Fig. S3(a) to S4(a)). Possible explanations were the occurrence of specific low-frequency rhythms in different regions depending on the specific physiological tasks. For example, γ amplitude

was modulated by θ rhythm in anterior frontal and temporal sites during an auditory task, whereas γ oscillations were conditioned on the α phase in the occipital region for a visual task [34]. Likewise, our findings also revealed that a strong high β-γ PAC of fear emerges in the F4 channel (Fig. 8(d)), which supported the contribution of β and γ bands in the arousal of fear [35].

In Fig. 6(a), the emotion of calmness shows a high δ/θ-α PAC, implying that α activity in the anterior frontal region is a potential feature for neutral emotion. Our finding resembles that of past works in showing α power elevates under the resting state in neutral emotional state, which facilitated calmness and mind/body integration [36]. While receiving neutral (video) stimuli, the subjects tended to calm down, along with the increased α responses. On the other hand, for the emotion of calmness, we found that with the high amplitude-given frequency (γ band) fixed, if the driving phase frequency increased, the coupling strength increased, and the brain area showing the strongest coupling shifted from the anterior-frontal to the frontal-central regions (left panels from Fig. 6(c) to (e)). This finding extends the findings by Kong, who suggested higher the synchronization level shifted from the prefrontal toward the occipital lobe with increasing phase frequency under relaxing state [37]. Hence, we speculate that phase modulations for a neutral emotional state differ in frequencies across brain regions, briefly slow waves occur in the anterior-frontal/frontal lobes, while fast activities in the central/lateral area.

Additionally, our findings revealed the asymmetric frontal PAC on emotional response; for example, excitement shows greater right fronto-central (F4 and FC6) α-β PACs than those of homologous left positions, whereas disgust presents stronger PACs in the left anterior-frontal region (Fig. S2(b)), which seems opposite to power asymmetry in brain hemispheres reported in the literature. That is, greater left frontal activity was related to a positive tendency [38], whereas increased right lobe activity presented withdrawal motivation [39], indicating that the activation of the brain region may inhibit the information interaction. Noted that hypoactivity does not necessarily correlate to cross-coupling. However, the relationship between specific-side frontal lobe hypoactivity and PAC strength remains unclear. Our results show that frontal asymmetry is linked with α-related PACs, and amusement and excitement present opposite dominant sides with high β-γ frontal PAC (Fig. 8(d)), which indicates that PAC asymmetry may be only a trait of a specific emotion.

In terms of methodology, we introduced the VMD method to PAC to improve cross-coupling analyses of brain dynamics. VMD is a completely nonrecursive algorithm based on the Fourier domain, in which each pattern is iteratively updated in the frequency domain. A narrowband Wiener filter corresponding to the estimation of the center frequency of the current mode is used to estimate the signal residuals of all other modes. The center of gravity of the mode power spectrum is re-estimated with the center frequency. This solution process not only preserves both the intra- and interwave characteristics of the time series for each mode but also greatly improves the mode mixing of EMD. In this study, the proposed VPAC estimates the coupling intensity of simulations by capturing cross-coupling between irregular oscillators around precise center frequencies, avoiding the occurrence of spurious PACs due to mode mixing or harmonics to ensure the faithfulness of biomarkers. We also applied the phase domain complexity (PDC) proposed by Aydın to compare the characteristic of different emotions [40]. The complexities of the neutral emotional state were significantly higher than those of positive/negative states (Fig. S5(a)), which further supports the capability of transmitting information during the neutral state is the highest with γ-amplitude-related PAC. Overall, our results support the VPAC method as a reliable tool to extract a wide spectrum of phase and amplitude modulations from physiological oscillations when the intensity of coupling is assessed accurately.

One limitation of the current study could be our focus on the intrachannel PAC over the frontal/prefrontal area, the interactions between electrodes and the other brain regions (e.g., central, temporal, and parietal lobes) are beyond our scope. Another limitation of this work may be the type of emotions in neutral and positive emotional states is not adequate, thus cross-frequency interactions with more emotional dynamics require further exploration.

V. Conclusion

In this study, we proposed a novel framework in variational PAC to investigate the interacting brain rhythm in emotion processing. Both nonlinear and nonstationary synthetic signals were devised to assess the validity of this approach. The variational PAC outperforms EEMD/IF-dependent PAC in identifying the high-frequency amplitude oscillations depending on the lower frequency phase. Our results indicate that the γ amplitude is critical in emotional processing, of which the coupling intensity with neutral emotional state is the strongest in the frontal and frontal-central areas, whereas for couplings with low-frequency amplitude modulation, the coupling intensity either with the positive or negative emotional state is stronger than that of the neutral emotion in the same areas. On the other hand, with the increase of the phase-given driving frequency, the γ-amplitude-related coupling strength increased, and the strongest coupling intensity shifted from the anterior-frontal to the frontal-central area. Furthermore, the α activity in the AF brain area contributed highly to the neutral emotion. As per our results, we suggest the proposed variational PAC as an effective and reliable method for assessing emotion brain networks.

References

[1] B. Kılıç and S. Aydın, "Classification of contrasting discrete emotional states indicated by EEG based graph theoretical network measures," *Neuroinformatics*, vol. 20, no. 4, pp. 863–877, Oct. 2022.
[2] P. Ekman et al., "Universals and cultural differences in the judgments of facial expressions of emotion," *J. Pers. Soc. Psychol.*, vol. 53, no. 4, pp. 712–717, Oct. 1987.
[3] J. A. Russell, "A circumplex model of affect," *J. Pers. Soc. Psychol.*, vol. 39, no. 6, pp. 1161–1178, Dec. 1980.
[4] A. Mehrabian, "Pleasure-arousal-dominance: A general framework for describing and measuring individual differences in temperament," *Curr. Psychol.*, vol. 14, pp. 261–292, Dec. 1996.
[5] L. Pessoa, "How do emotion and motivation direct executive control," *Trends Cogn. Sci.*, vol. 13, pp. 160–166, Apr. 2009.
[6] B. Voytek et al., "Oscillatory dynamics coordinating human frontal networks in support of goal maintenance," *Nature Neurosci.*, vol. 18, no. 9, pp. 1318–1324, Sep. 2015.

[7] M. Soleymani, S. Asghari-Esfeden, Y. Fu, and M. Pantic, "Analysis of EEG signals and facial expressions for continuous emotion detection," *IEEE Trans. Affect. Comput.*, vol. 7, no. 1, pp. 17–28, Jan.–Mar. 2016.

[8] W.-L. Zheng, J.-Y. Zhu, and B.-L. Lu, "Identifying stable patterns over time for emotion recognition from EEG," *IEEE Trans. Affect. Comput.*, vol. 10, no. 3, pp. 417–429, Jul.–Sep. 2019.

[9] D. Sammler, M. Grigutsch, T. Fritz, and S. Koelsch, "Music and emotion: Electrophysiological correlates of the processing of pleasant and unpleasant music," *Psychophysiology*, vol. 44, no. 2, pp. 293–304, Feb. 2007.

[10] S. Aydın, "Cross-validated adaboost classification of emotion regulation strategies identified by spectral coherence in resting-state," *Neuroinformatics*, vol. 20, no. 3, pp. 627–639, Jul. 2022.

[11] J. Sorinas, J. C. Fernandez-Troyano, J. M. Ferrandez, and E. Fernandez, "Cortical asymmetries and connectivity patterns in the valence dimension of the emotional brain," *Int. J. Neural Syst.*, vol. 30, no. 5, May 2020, Art. no. 2050021.

[12] W. Shi, C.-H. Yeh, and Y. Hong, "Cross-frequency transfer entropy characterize coupling of interacting nonlinear oscillators in complex systems," *IEEE Trans. Biomed. Eng.*, vol. 66, no. 2, pp. 521–529, Feb. 2019.

[13] W. Shi, C.-H. Yeh, and J. An, "Cross-channel phase-amplitude transfer entropy conceptualize long-range transmission in sleep: A case study," in *Proc. IEEE 41st Annu. Int. Conf. IEEE Eng. Med. Biol. Soc.*, 2019, pp. 4048–4051.

[14] A. Hyafil, A.-L. Giraud, L. Fontolan, and B. Gutkin, "Neural cross-frequency coupling: Connecting architectures, mechanisms, and functions," *Trends Neurosci.*, vol. 38, no. 11, pp. 725–740, Nov. 2015.

[15] S. Amemiya and A. D. Redish, "Hippocampal theta-gamma coupling reflects state-dependent information processing in decision making," *Cell Rep.*, vol. 22, no. 12, pp. 3328–3338, Mar. 2018.

[16] L. Jin, W. Shi, C. Zhang, and C. H. Yeh, "Frequency nesting interactions in the subthalamic nucleus correlate with the step phases for Parkinson's disease," *Front. Physiol.*, vol. 13, Apr. 2022, Art. no. 890753.

[17] C. H. Yeh et al., "Quantifying spasticity with limited swinging cycles using pendulum test based on phase amplitude coupling," *IEEE Trans. Neural Syst. Rehabil. Eng.*, vol. 24, no. 10, pp. 1081–1088, Oct. 2016.

[18] R. V. Chacko et al., "Distinct phase-amplitude couplings distinguish cognitive processes in human attention," *NeuroImage*, vol. 175, pp. 111–121, Jul. 2018.

[19] Y. Wang, W. Shi, and C.-H. Yeh, "A novel measure of cardiopulmonary coupling during sleep based on the synchrosqueezing transform algorithm," *IEEE J. Biomed. Health Inform.*, early access, Jan. 17, 2023, doi: 10.1109/JBHI.2023.3237690.

[20] N. Huang et al., "The empirical mode decomposition and the Hilbert spectrum for nonlinear and non-stationary time series analysis," *Proc. Roy. Soc. London. Ser. A: Math., Phys. Eng. Sci.*, vol. 454, no. 1971, pp. 903–995, Mar. 1998.

[21] B. Pittman-Polletta, W. H. Hsieh, S. Kaur, M. T. Lo, and K. Hu, "Detecting phase-amplitude coupling with high frequency resolution using adaptive decompositions," *J. Neurosci. Methods*, vol. 226, pp. 15–32, Apr. 2014.

[22] L. Lin, Y. Wang, and H. Zhou, "Iterative filtering as an alternative algorithm for empirical mode decomposition," *Adv. Adaptive Data Anal.*, vol. 1, pp. 543–560, Oct. 2009.

[23] K. Dragomiretskiy and D. Zosso, "Variational mode decomposition," *IEEE Trans. Signal Process.*, vol. 62, no. 3, pp. 531–544, Feb. 2014.

[24] C. H. Yeh and W. Shi, "Identifying phase-amplitude coupling in cyclic alternating pattern using masking signals," *Sci. Rep.*, vol. 8, no. 1, Feb. 2018, Art. no. 2649.

[25] S. Katsigiannis and N. Ramzan, "DREAMER: A database for emotion recognition through EEG and ECG signals from wireless low-cost off-the-shelf devices," *IEEE J. Biomed. Health Inform.*, vol. 22, no. 1, pp. 98–107, Jan. 2018.

[26] L. Aftanas, N. V. Reva, A. A. Varlamov, S. V. Pavlov, and V. P. Makhnev, "Analysis of evoked EEG synchronization and desynchronization in conditions of emotional activation in humans: Temporal and topographic characteristics," *Neurosci. Behav. Physiol.*, vol. 34, no. 8, pp. 859–867, Oct. 2004.

[27] A. B. Tort, R. Komorowski, H. Eichenbaum, and N. Kopell, "Measuring phase-amplitude coupling between neuronal oscillations of different frequencies," *J. Neurophysiol.*, vol. 104, no. 2, pp. 1195–1210, Aug. 2010.

[28] D. Aldous and P. Diaconis, "Shuffling cards and stopping times," *Amer. Math. Monthly*, vol. 93, no. 5, pp. 333–348, May 1986.

[29] C. H. Yeh, M. T. Lo, and K. Hu, "Spurious cross-frequency amplitude–amplitude coupling in nonstationary, nonlinear signals," *Phys. A*, vol. 454, pp. 143–150, Jul. 2016.

[30] C. Zhang, W. Shi, and C. H. Yeh, "Investigating variational phase-amplitude coupling in EEG-based emotion recognition," in *Proc. 10th Int. IEEE/EMBS Conf. Neural Eng.*, 2021, pp. 150–153.

[31] F. Bi, X. Li, C. Liu, C. Tian, T. Ma, and X. Yang, "Knock detection based on the optimized variational mode decomposition," *Measurement*, vol. 140, Jul. 2019, Art. no. 115537400.

[32] A. K. Engel and W. Singer, "Temporal binding and the neural correlates of sensory awareness," *Trends Cogn. Sci.*, vol. 5, no. 1, pp. 16–25, Jan. 2001.

[33] Y. Li, D. Cao, L. Wei, Y. Tang, and J. Wang, "Abnormal functional connectivity of EEG gamma band in patients with depression during emotional face processing," *Clin. Neurophysiol.*, vol. 126, no. 11, pp. 2078–2089, Nov. 2015.

[34] R. T. Canolty and R. T. Knight, "The functional role of cross-frequency coupling," *Trends Cogn. Sci.*, vol. 14, no. 11, pp. 506–515, Nov. 2010.

[35] N. Masood and H. Farooq, "Investigating EEG patterns for dual-stimuli induced human fear emotional state," *Sensors*, vol. 19, no. 3, Jan. 2019, Art. no. 522.

[36] W. O. Ismail, M. Hanif, S. B. Mohamed, N. Hamzah, and Z. I. Rizman, "Human emotion detection via brain waves study by using electroencephalogram (EEG)," *Int. J. Adv. Sci. Eng. Inf. Technol.*, vol. 6, no. 6, pp. 1005–1011, Dec. 2016.

[37] W. Kong, X. Song, and J. Sun, "Emotion recognition based on sparse representation of phase synchronization features," *Multimedia Tools Appl.*, vol. 80, pp. 21203–21217, Mar. 2021.

[38] W. Zheng, "Multichannel EEG-based emotion recognition via group sparse canonical correlation analysis," *IEEE Trans. Cogn. Devlop. Syst.*, vol. 9, no. 3, pp. 281–290, Sep. 2017.

[39] I. Papousek, E. M. Weiss, G. Schulter, A. Fink, E. M. Reiser, and H. K. Lackner, "Prefrontal EEG alpha asymmetry changes while observing disaster happening to other people: Cardiac correlates and prediction of emotional impact," *Biol. Psychol.*, vol. 103, pp. 184–194, Dec. 2014.

[40] S. Aydin, "Deep learning classification of neuro-emotional phase domain complexity levels induced by affective video film clips," *IEEE J. Biomed. Health Inform.*, vol. 24, no. 6, pp. 1695–1702, Jun. 2020.